ULTRAFAST OPTICS

Ultrafast Kapitza-Dirac effect

Kang Lin[1,2]*, Sebastian Eckart[2], Hao Liang[3], Alexander Hartung[2], Sina Jacob[2], Qinying Ji[2,4], Lothar Ph. H. Schmidt[2], Markus S. Schöffler[2], Till Jahnke[5], Maksim Kunitski[2], Reinhard Dörner[2]*

Similar to the optical diffraction of light passing through a material grating, the Kapitza-Dirac effect occurs when an electron is diffracted by a standing light wave. In its original description, the effect is time independent. Here, we extended the Kapitza-Dirac effect to the time domain. By tracking the spatiotemporal evolution of a pulsed electron wave packet diffracted by a 60-femtosecond (where one femtosecond = 10^{-15} seconds) standing wave pulse in a pump-probe scheme, we observed time-dependent diffraction patterns. The fringe spacing in the observed pattern differs from that generated by the conventional Kapitza-Dirac effect. By exploiting this time-resolved diffraction scheme, we can access the time evolution of the phase properties of a free electron and potentially image ionic potentials and electronic decoherences.

Shortly after the wave nature of electrons was demonstrated by diffracting an electron beam at a periodic crystal structure (*1*), Kapitza and Dirac suggested that an electron beam can also be diffracted by an immaterial standing light wave (*2*). Today, this is referred to as the Kapitza-Dirac effect (*3*). It was shown that this diffraction occurs due to the stimulated Compton back-scattering of photons in the standing wave. During this process, n times twice the photon momentum $\hbar k_\gamma$ is imparted onto the electron, causing the deflection of the electron beam to discrete angles. Unlike this particle perspective of photon scattering, the standing wave can be thought of as a spatially periodic ponderomotive potential that leads to diffraction of the electron wave packet (*3*). In matter optics, the Kapitza-Dirac effect is used for the manipulation of matter waves. For instance, a standing light wave can serve as a coherent beam splitter for particle bunches, including electrons, ions, atoms, and molecules (*3*–*6*). Such a matter splitter is an essential part of particle interferometers (*7*), which have many applications ranging from extremely sensitive studies of gravitational effects (*8*) to the generation of spin-polarized electrons (*9*). Further, laser fields are routinely used for shaping electron bunches in electron microscopy (*10*–*16*). Despite the existing body of theoretical work (*17*–*19*), the conventional Kapitza-Dirac effect on electrons was not observed until 2001 (*20*) because of the experimental challenges mainly related to the overall weakness of the effect. In that experiment, a narrowly collimated electron beam produced by an electron gun was used. The electrons traveled through a standing light wave, which was formed by two counterpropagating laser beams. In the final electron momentum spectrum, discrete diffraction peaks spaced by two-photon momenta, $2\hbar k_\gamma$, were observed (*20*, *21*) (Fig. 1A).

The advent of the ultrafast laser technology provides the opportunity to address the dynamics of the Kapitza-Dirac photon scattering in an ultrafast pump-probe experiment and explore the time dependence of the electron diffraction. In addition, strong laser fields can be used for the production of electrons through ionizing neutral atoms or molecules, which are then subject to the Kapitza-Dirac effect in the experiment. Electrons released by such laser fields from atoms or molecules have specific properties that are different from those produced by an electron gun. The former can be considered as a coherent electron wave packet with a broad distribution in momentum space, and the latter can be approximated as a plane wave with a momentum-space distribution close to a delta function. The early attempts (*22*) used two counterpropagating, 100-ps (where 1 ps = 10^{-12} s) laser pulses to form a standing light wave. The pulsed standing wave ionized individual atoms in the gas phase, setting the electrons free and subsequently diffracting them. As a result of a very high photon-scattering rate in the intense light field, the measured electron angular emission distribution consisted of two peaks with a spacing corresponding to thousands of photon momenta. This is also referred to as "rainbow" scattering (*19*) or channeling (*23*). No peaks spaced by two-photon momenta were observed [see (*24*) for theoretical modeling predicting such interference fringes]. In a later experiment, a 55-fs standing wave was used to scatter neutral atoms (*25*). However, neither of these experiments observed interference fringes, nor did they have access to the temporal properties of the diffraction process.

Fully time-resolved experiment on the Kapitza-Dirac effect

The concept of our experiment is illustrated in Fig. 1B. An electron wave packet was released from a xenon atom upon strong-field ionization using a highly intense, pulsed standing light wave (pump pulse). After a variable time delay, a weaker, non-ionizing, femtosecond standing light wave (probe pulse) was applied to diffract the emitted electron wave packet. The pump and the probe pulses were generated by a commercial Ti:Sapphire laser system (Coherent Legend Elite Duo, 25 fs, 800 nm, 10 kHz) by focusing two counterpropagating laser pulses into the same target volume (*26*), where they were finally stretched to ~60 fs. Using a standing wave as the pump locks the birth position of the electron wave packet relative to the field maxima of the probe standing wave (see the supplementary materials). The three-dimensional (3D) momenta of the electrons were measured using a COLd Target Recoil Ion Momentum Spectroscopy (COLTRIMS) reaction microscope (*27*, *28*).

With this experimental arrangement, we observed time-dependent interference fringes in the electron momentum distribution. The fringe spacing was decreased continuously by increasing the time delay between the pump and probe pulses. This observation is different from that of the conventional Kapitza-Dirac effect, where the diffraction pattern shows a constant spacing of two-photon momenta. The corresponding results depict the measured 2D electron momentum distribution along the laser polarization (z axis) and propagation directions (x axis) for various time delays (Fig. 2). For the sake of visibility, a gating of $|p_y| > 0.1$ a.u. (atomic units are used unless stated otherwise) was applied to the dataset to remove the Coulomb-focusing-induced distortions around the center of the 3D momentum distribution (*29*, *30*). The y axis points along the direction of the gas jet. As a reference, Fig. 2A shows the momentum distribution recorded at negative time delay of –1 ps. In this case, the probe pulse arrives before the pump pulse such that the electron wave packet, which is released by the pump pulse, does not experience diffraction by the standing wave. The 2D momentum distribution extends along the polarization direction (p_z) of the pump pulse resulting from the acceleration of electrons by the pump pulse's electric field. Along the light-propagation direction (p_x), the electron momentum distribution is much narrower because it is determined solely by the initial velocity distribution of the electrons upon tunneling. The distribution is similar to the extensively studied momentum

[1]School of Physics, Zhejiang Key Laboratory of Micro-Nano Quantum Chips and Quantum Control, Zhejiang University, Hangzhou 310058, China. [2]Institut für Kernphysik, Goethe-Universität, 60438 Frankfurt am Main, Germany. [3]Max Planck Institute for the Physics of Complex Systems, 01187 Dresden, Germany. [4]Center for Ultrafast Science and Technology, School of Chemistry and Chemical Engineering, Shanghai Jiao Tong University, Shanghai 200240, China. [5]Max-Planck-Institut für Kernphysik, 69117 Heidelberg, Germany.
*Corresponding author. Email: klin@zju.edu.cn (K.L.); doerner@atom.uni-frankfurt.de (R.D.)

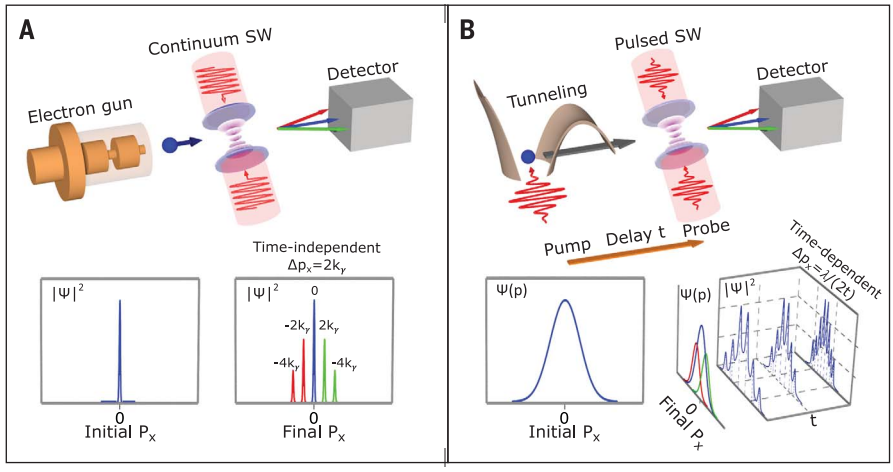

Fig. 1. Momentum space perspective of the conventional and the ultrafast Kapitza-Dirac effects. (**A**) The conventional Kapitza-Dirac effect describes the diffraction of a plane electron wave that can be represented as a delta function in momentum space. Thus, the width of the momentum distribution is much narrower than two-photon momenta $2k_\gamma$. In a standing light wave, stimulated Compton backscattering of photons shifts this narrow momentum distribution by $\pm 2nk_\gamma$, where n is an integer. The resulting regularly spaced peak structure in momentum space is time independent. (**B**) By contrast, for the ultrafast Kapitza-Dirac effect, the stimulated Compton backscattering transfers the momentum to an electron wave packet that has a very broad momentum distribution. The Compton backscattering occurs during a short time interval (femtoseconds) and at a variable time delay after the birth of the wave packet. The interference between the original (blue Gaussian) and the momentum-shifted (red and green Gaussians) wave packets leads to time-dependent fringes in momentum space.

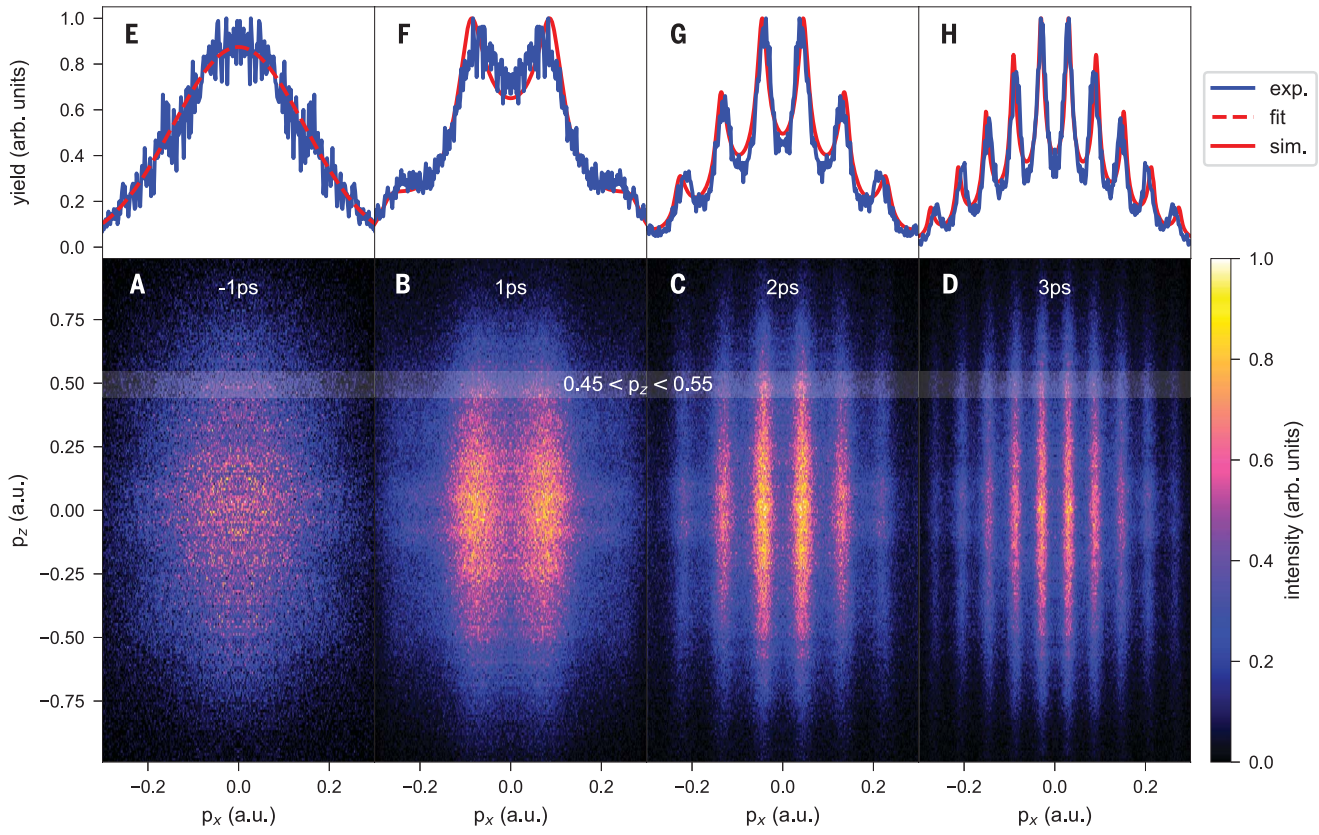

Fig. 2. Observation of the ultrafast Kapitza-Dirac effect. (**A** to **D**) Experimentally measured momentum distributions of the electron that is released upon strong-field ionization of xenon atoms in a pulsed standing light wave (800 nm, 60 fs, 1.0×10^{14} W/cm^2). The ionizing pulse is followed by a weak standing light wave pulse (0.4×10^{14} W/cm^2) that acts as a probe pulse. The probe pulse is attenuated such that it cannot lead to the liberation of bound electrons and thus only serves as a diffraction grating. Vertical axis shows the electron momentum along the polarization direction (p_z). Horizontal axis shows the electron momentum along the light-propagation direction (p_x). Panels (A) to (D) show the data taken for different time delays of −1, 1, 2, and 3 ps, respectively. (**E** to **H**) 1D momentum distribution along the light-propagation axis by selecting the range of p_z between (0.45, 0.55) atomic units [shaded areas in (A) to (D)]. The dashed curve in (E) is obtained by fitting a Gaussian distribution. The solid curves in (F) to (H) show results from numerically propagating a 1D electron wave packet followed by the interaction with a standing wave at different time delays.

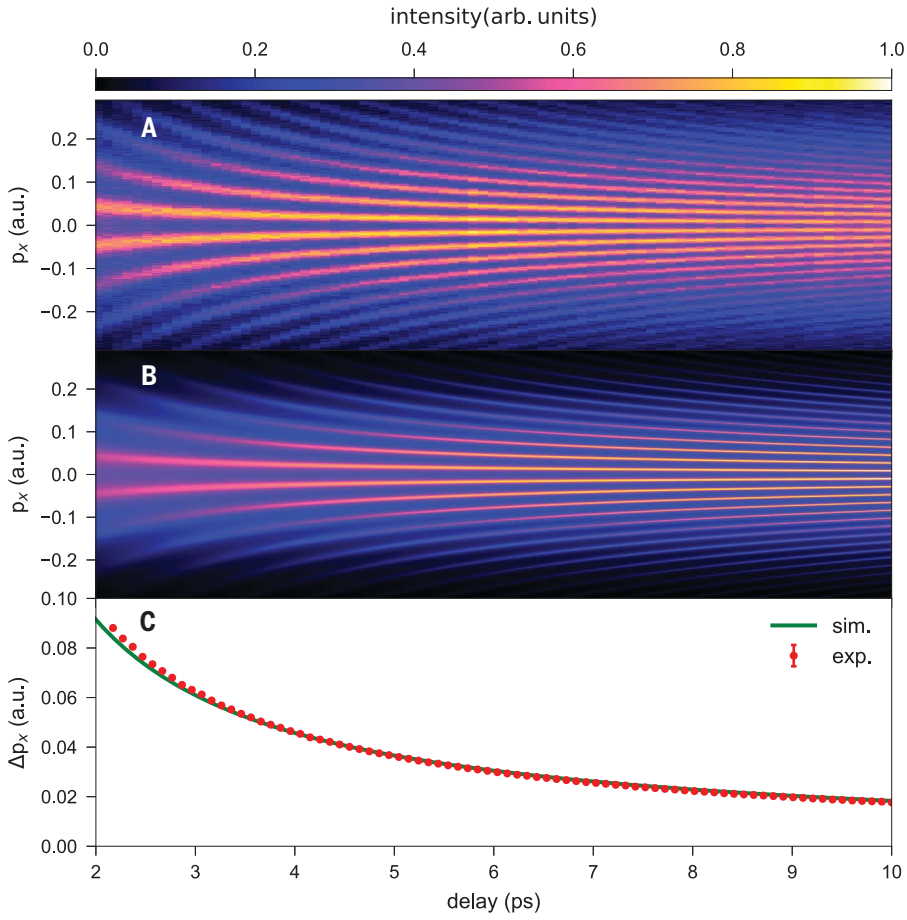

Fig. 3. Diffraction pattern as a function of time delay. (**A** and **B**) Measured (A) and simulated (B) electron momentum distribution along p_x for light pulses as in Fig. 2 as a function of the time delay between ionization (by the pump pulse) and probing by the non-ionizing standing light wave (probe pulse). The data are integrated over $|p_y|$ >0.1 a.u. (**C**) Fitted diffraction spacing from (A) as a function of the time delay. The solid curve is obtained from simulations in full analogy to the experiment.

distribution of electrons released by tunnel ionization using a single traveling femtosecond laser pulse (*31*). The Kapitza-Dirac effect manifests itself in the periodic vertical fringes, i.e., an intensity modulation along the light-propagation direction (horizontal axes in Fig. 2). At a negative pump-probe delay (Fig. 2A), we found along this direction a close to Gaussian distribution centered at zero momentum with a full width at half-maximum (FWHM) of ~0.25 a.u. At positive time delays (Fig. 2, B to D), the electron momentum distribution turned into fringe patterns in the light-propagation direction, and the spacing between diffraction fringes decreased with increasing time delay (Fig. 2, F to H). Specifically, the spacing between the diffraction peaks at 1, 2, and 3 ps was ~0.18, 0.09, and 0.06 a.u., respectively. To find a quantitative relation between the diffraction spacing and the time delay, we performed a continuous scan of the pump-probe delay from 2 to 10 ps. Figure 3A clearly shows that the spacing between the diffraction fringes decreased continuously with increasing time delay. We found that the spacing between the diffraction peaks equals one half the wavelength of the standing light wave λ_{SW} times the electron mass m_e (with m_e = 1 in atomic units) divided by the time delay, i.e.

$$\Delta p_x = m_e \frac{\lambda_{SW}}{2t} \quad (1)$$

This result was unexpected because the conventional Kapitza-Dirac effect is time independent. Hereafter, we refer to this newly observed phenomenon as the "ultrafast Kapitza-Dirac effect."

Numerical modeling

To understand the underlying physics of the ultrafast Kapitza-Dirac effect, we numerically propagated a 1D electron wave packet, followed by interaction with the pulsed standing wave (*28*). We started with an initial electron wave packet defined by the distribution observed for the negative time delay (Fig. 2E) and with a width of ~0.25 a.u. in momentum space. This is a very broad distribution compared with the transverse momentum distribution of a collimated electron beam (which is often even approximated by a delta function in momentum space). Specifically, in (*20*), the electron beam had a momentum distribution with a width of 2.2×10^{-4} a.u. along the light-propagation direction. Subsequently, the initial electron wave packet evolved under field-free conditions. At different time delays, we applied an ultrashort spatially periodic potential (which mimics the ponderomotive potential of the probe pulse) to diffract the electron wave packet. The simulated momentum distributions show fringes (Figs. 2 and 3) that agree very well with the experimental observation and its time-domain behavior.

The ultrafast Kapitza-Dirac effect can be conceptionally understood as an interference between the initial electron wave packet and a replica of the electron wave packet that has been shifted in momentum space by $2k_\gamma$ resulting from stimulated Compton backscattering of the photons of the probe pulse. Although the initial electron wave packet evolves under field-free conditions [thus, accompanied with a phase evolution of $\varphi_e(t) = p_x^2 t/2$], the altered electrons experience the aforementioned $2k_\gamma$ recoil along the light-propagation direction when interacting with the standing wave. Accordingly, this interaction leads to a momentum-shifted electron wave packet with an accompanying phase of $\varphi'_e(t) = \left(p_x \pm 2k_\gamma\right)^2 t/2 + \varphi_{SW}$, where φ_{SW} encodes the relative phase of the standing wave with respect to the initial electron wave packet (*28*). The tiny change of energy of the electron is compensated by an equivalent change of the photon energy upon scattering, which is within the bandwidth of the short pulse. In our case, $\varphi_{SW} = \frac{\pi}{2}$. The initial and shifted wave packets interfere constructively when the phase difference is $\Delta\varphi_e = \varphi'_e - \varphi_e = 2n\pi$. Thus, the peaks in the final electron momentum distribution are expected to be located at $(p_x)_n \approx \frac{n\pi}{tk_\gamma} = \left(n + \frac{1}{2}\right)\frac{\lambda_{SW}}{2t}$, resulting in a modulation spacing of $\Delta p_x = \frac{\lambda_{SW}}{2t}$.

Concluding remarks

The ultrafast Kapitza-Dirac effect differs fundamentally from the conventional Kapitza-Dirac effect. In momentum space, the latter generates extremely narrow (delta-function-like) side bands in momentum space. Because these sidebands and the original momentum distribution of the electron do not overlap, an interference of these contributions is not possible. In the case of the ultrafast Kapitza-Dirac effect, however, the momentum shift of $2k_\gamma$ is much smaller than the width of the initial electron wave packet, which enables an interference of the initial and scattered contribution (Figs. 2 and 3). The observed interference fringes not only provide insight

into the temporal dynamics of the studied light-matter interaction, but we also envision that the ultrafast Kapitza-Dirac effect can be used as a powerful interferometer to measure phase gradients of free electrons in general, an observable that is otherwise inaccessible using state-of-the-art electron spectroscopy. Techniques such as velocity map imaging, dispersive electron analyzers, and COLTRIMS reaction microscopes routinely access the amplitude of electron wave packets. Approaches to learning about the phase of photoelectrons, such as RABBITT (Reconstruction of Attosecond Beating by Interference of Two-photon Transitions) (*32*, *33*) or HASE (Holographic Angular Streaking of Electrons) (*34*, *35*), rely on intercepting the photoelectron's creation mechanism. By contrast, the ultrafast Kapitza-Dirac effect acts as an electron interferometer that reads out phase information long after the ionization event, leaving the ionization process undistorted. The interference fringes shown in Figs. 2 and 3 for positive time delays are therefore the result of probing a freely propagating electron and accessing its quantum-phase properties. Conversely, the contrast of the diffraction fringes can serve as a probe for the coherence of the electron wave packet. Thus, the ultrafast Kapitza-Dirac effect could be used to trace the time dependence of decoherence caused by interaction with an environment such as a large molecule or a neighboring metal cluster surface (*36*, *37*). Possible applications of such pulsed Kapitza-Dirac interferometers are investigating (i) phase entanglement between several electrons or between electrons and ions, (ii) electrons released from surfaces, or (iii) chiral electron wave packets, tracking the origin of their chirality as they emerge from chiral molecules.

REFERENCES AND NOTES

1. C. Davisson, L. H. Germer, *Nature* **119**, 558–560 (1927).
2. P. L. Kapitza, P. A. M. Dirac, *Math. Proc. Camb. Philos. Soc.* **29**, 297–300 (1933).
3. H. Batelaan, *Rev. Mod. Phys.* **79**, 929–941 (2007).
4. P. L. Gould, G. A. Ruff, D. E. Pritchard, *Phys. Rev. Lett.* **56**, 827–830 (1986).
5. O. Nairz, B. Brezger, M. Arndt, A. Zeilinger, *Phys. Rev. Lett.* **87**, 160401 (2001).
6. B. A. Stickler, M. Diekmann, R. Berger, D. Wang, *Phys. Rev. X* **11**, 031056 (2021).
7. D. M. Giltner, R. W. McGowan, S. A. Lee, *Phys. Rev. Lett.* **75**, 2638–2641 (1995).
8. X. Wu *et al*., *Sci. Adv.* **5**, eaax0800 (2019).
9. M. M. Dellweg, C. Müller, *Phys. Rev. Lett.* **118**, 070403 (2017).
10. A. H. Zewail, *Science* **328**, 187–193 (2010).
11. H. Müller *et al*., *New J. Phys.* **12**, 073011 (2010).
12. M. Kozák, N. Schönenberger, P. Hommelhoff, *Phys. Rev. Lett.* **120**, 103203 (2018).
13. S. A. Koppell *et al*., *Ultramicroscopy* **207**, 112834 (2019).
14. O. Schwartz *et al*., *Nat. Methods* **16**, 1016–1020 (2019).
15. K. Wang *et al*., *Nature* **582**, 50–54 (2020).
16. M. C. Chirita Mihaila *et al*., *Phys. Rev. X* **12**, 031043 (2022).
17. R. Gush, H. P. Gush, *Phys. Rev. D Part. Fields* **3**, 1712–1721 (1971).
18. M. V. Fedorov, *Opt. Commun.* **12**, 205–209 (1974).
19. H. Batelaan, *Contemp. Phys.* **41**, 369–381 (2000).
20. D. L. Freimund, K. Aflatooni, H. Batelaan, *Nature* **413**, 142–143 (2001).
21. D. L. Freimund, H. Batelaan, *Phys. Rev. Lett.* **89**, 283602 (2002).
22. P. H. Bucksbaum, D. W. Schumacher, M. Bashkansky, *Phys. Rev. Lett.* **61**, 1182–1185 (1988).
23. C. Salomon, J. Dalibard, A. Aspect, H. Metcalf, C. Cohen-Tannoudji, *Phys. Rev. Lett.* **59**, 1659–1662 (1987).
24. X. Li *et al*., *Phys. Rev. Lett.* **92**, 233603 (2004).
25. S. Eilzer, H. Zimmermann, U. Eichmann, *Phys. Rev. Lett.* **112**, 113001 (2014).
26. A. Hartung *et al*., *Nat. Phys.* **15**, 1222–1226 (2019).
27. R. Dörner *et al*., *Phys. Rep.* **330**, 95–192 (2000).
28. See the supplementary materials.
29. T. Brabec, M. Y. Ivanov, P. B. Corkum, *Phys. Rev. A* **54**, R2551–R2554 (1996).
30. A. Ludwig *et al*., *Phys. Rev. Lett.* **113**, 243001 (2014).
31. S. V. Popruzhenko, *J. Phys. At. Mol. Opt. Phys.* **47**, 204001 (2014).
32. P. M. Paul *et al*., *Science* **292**, 1689–1692 (2001).
33. H. G. Muller, *Appl. Phys. B* **74**, s17–s21 (2002).
34. S. Eckart, *Phys. Rev. Res.* **2**, 033248 (2020).
35. D. Trabert *et al*., *Nat. Commun.* **12**, 1697 (2021).
36. P. Sonnentag, F. Hasselbach, *Phys. Rev. Lett.* **98**, 200402 (2007).
37. N. Kerker, R. Röpke, L. M. Steinert, A. Pooch, A. Stibor, *New J. Phys.* **22**, 063039 (2020).
38. Data for: K. Lin *et al*., Ultrafast Kapitza-Dirac effect, Zenodo (2024); https://doi/10.5281/zenodo.10617990.

ACKNOWLEDGMENTS

We thank C. Lu and J. Jiang for figure plotting and P. He and F. He for fruitful discussions. **Funding:** This work was supported by the DFG (German Research Foundation). S.E. was supported by the DFG through Priority Programme SPP 1840 QUTIF. **Author contributions:** K.L., S.E., A.H., S.J., Q.J., L.Ph.H.S., M.S.S., T.J., M.K., and R.D. performed the experiments. K.L., S.E., M.K., and R.D. analyzed the data. M.K. and H.L. performed the simulations. All authors contributed to writing the manuscript. **Competing interests:** The authors declare no competing interests. **Data and materials availability:** All data are available in the manuscript or the supplementary materials and have been deposited at Zenodo (*38*).

SUPPLEMENTARY MATERIALS

science.org/doi/10.1126/science.adn1555
Materials and Methods
Supplementary Text
Figs. S1 to S3

Submitted 27 November 2023; accepted 20 February 2024
10.1126/science.adn1555